

Interplay between Spin and Orbital Angular Momenta in Tightly Focused Higher-Order Poincaré Sphere Beams

Panpan Yu, Yifan Liu, Ziqiang Wang, Yinmei Li, and Lei Gong*

Spin-orbit interactions (SOIs) of light in tight focusing systems have gained much attention due to the potential applications in optical trapping and microscopy. SOI effects strongly affect the distributions and properties of focal fields, which are determined by the polarization and spatial degrees of freedom of incoming light. Remarkably, structured light fields exhibit SOI phenomena with complex behaviors. Here the SOIs in the tightly focused higher-order Poincaré sphere beams that simultaneously contain vortex phase front and higher polarization orders are theoretically studied. The interplay between spin and orbital angular momenta in the focused field is revealed, and the amount of spin-orbit conversion is found to be determined by the angular momentum of the incident field and the focusing system. In particular, based on the superposition of two circular polarization vortex bases, a general description of the interplay between spin and orbital parties is provided, paving a way to arbitrarily controlling the SOIs in nonparaxial fields. The findings are expected to deepen the understanding of SOIs that play a critical role in classical and quantum optics.

spin-dependent effects in focused or scattered fields,^[9–12] spin-controlled shaping of light using metasurfaces, and robust spin-directional coupling via evanescent near fields.^[13–15] Recently, SOI effects have been widely applied in classical and quantum optics. For example, SOI-based optical nano-devices enable arbitrary, parallel control of light's phase and polarization as well as the temporal characteristics,^[16] allowing generation of structured light or plasmonic fields, and shaping ultrafast optical pulse.^[17] These SOI-enabled wavefront shaping techniques further benefit optical communications, holography and display, full-color computational imaging, full-Stokes polarization photography, and quantum state imaging.^[18–21] In the tight focusing and scattering systems, the SOI phenomena carry rich information about light interaction with matter that are highly

1. Introduction


Light can carry both spin and orbital angular momenta (AM), which are determined by light's polarization and spatial degrees of freedom (DOFs). The rotating electric fields in a circularly polarized beam produce spin angular momentum (SAM).^[1] and optical vortex beams with helical wavefronts carry orbital angular momentum (OAM).^[2] In paraxial fields, optical SAM and OAM are mutually independent and conserved under free-space propagation.^[3] By contrast, they can strongly couple with each other in nonparaxial fields.^[4] Actually, spin-orbit interactions (SOIs) are universal phenomena in optics and photonics especially at the subwavelength scales, such as the spin-Hall effects in inhomogeneous media and at optical interfaces.^[5–8]

attractive for optical nano-probing.^[22,23] For instance, a chiral dipolar scatter can recognize the vorticity of the incoming light field by detecting the focal optical chirality.^[22]

Because tight focusing is widely involved in applications such as optical trapping and microscopy,^[24–27] SOIs occurring in tight focusing systems have gained much attention recently.^[4,28] In these systems, SOI effects strongly affect the focal distributions and properties, which are determined by the polarization and spatial DOFs of incoming light. As a consequence, structured light fields under tight focusing exhibit unique SOI phenomena with complex behaviors. In a tightly focused circularly polarized field, SAM of incident light could be transformed into OAM in the focused field, which is termed as spin-to-orbit-conversion (SOC).^[29,30] Notably, the SOC can enable orbiting of isotropic particles trapped by a tightly focused nonvortex beam.^[31] Apart from SOC, the orbit-induced localized SAM, termed as local orbit-to-spin-conversion (OSC), can also occur under tight focusing. We have revealed in theory that localized OSC occurs in strong focusing of a linearly polarized Laguerre–Gaussian beam.^[32] Such a local OSC has been verified experimentally by the interaction of light carrying OAM with a chiral dipolar scatterer.^[22] The OSC was also found to occur in the tightly focused radially or azimuthally polarized vortex beams, which possess no SAM before being focused.^[33,34] Although the SOC and OSC have been observed separately, the interplay between SAM and OAM in the focused field has not been revealed so far, which may shed new insight on light–matter interactions.

Dr. P. Yu, Dr. Y. Liu, Dr. Z. Wang, Prof. Y. Li, Dr. L. Gong
Department of Optics and Optical Engineering
University of Science and Technology of China
Hefei 230026, China
E-mail: leigong@ustc.edu.cn

Prof. Y. Li
Hefei National Laboratory for Physical Sciences at the Microscale
University of Science and Technology of China
Hefei 230026, China

 The ORCID identification number(s) for the author(s) of this article can be found under <https://doi.org/10.1002/andp.202000110>

DOI: 10.1002/andp.202000110

In this paper, we theoretically study the interplay between SAM and OAM in tightly focused higher-order Poincaré sphere (HOP) beams that feature vortex phase front and higher-order polarization states simultaneously.^[35–37] The electric field distributions and local AM densities in the focused fields are analyzed, demonstrating the occurrence of both SOC and OSC for the focused HOP beams. In particular, the complex behaviors of the interconversion between the spin and orbital AM are revealed by studying various HOP beams with varying polarization and vortex phase in the incident field. The numerical results indicate that there exists an extra OAM transformed from the incident SAM under tight focusing. Also, the incident OAM can induce the occurrence of localized SAM in the focused field. When the incident field has SAM and OAM simultaneously, the complex interactions to each other happen in the focused field. In addition, the amount of spin-orbit conversion is found to be determined by the parameters of the incident field together with the high focusing system. Our findings are expected to deepen the understanding of SOI phenomena that play a critical role in classical and quantum optics. Further, the control of SAM and OAM in tightly focused HOP beams may bring new applications in light-matter interactions, such as optical trapping and super-resolution microscopy.

2. Theory

To study the interplay between SAM and OAM in tightly focused fields, we focus on structured light beams that possess both inhomogeneous polarization states and vortex phase front. Such kind of beams can be described using a higher-order Poincaré sphere (HOP), termed as HOP beams. Any state on the HOP can be realized by a superposition of two orthogonal states, that is, left and right-handed circularly polarized vortex beams. Mathematically, their complex amplitude is defined as

$$\begin{aligned} E(\rho, \varphi) = & \cos(\vartheta/2) \exp(-i\varphi/2) A(\rho) \exp(i\alpha\varphi) \hat{e}_L \\ & + \sin(\vartheta/2) \exp(i\varphi/2) A(\rho) \exp(i\beta\varphi) \hat{e}_R \end{aligned} \quad (1)$$

where \hat{e}_L and \hat{e}_R are the unit vectors of the two orthogonally circular bases. The two bases have the same amplitude $A(\rho)$ and different vortex phases. a and b are their topological charges, respectively. (ϑ, ϕ) represent the spherical coordinates. The coefficients of the two bases are coordinate dependent, which reads

$$\begin{aligned} A_L &= \cos(\vartheta/2) \exp(-i\phi/2), \\ A_R &= \sin(\vartheta/2) \exp(i\phi/2) \end{aligned} \quad (2)$$

Under the Cartesian coordinate system, the Stokes parameters ($S_1^{a,b}, S_2^{a,b}, S_3^{a,b}$) serve as the coordinates for the unified HOP ($S_0^{a,b} = |A_L|^2 + |A_R|^2 = 1$), which are defined as

$$\begin{aligned} S_1^{a,b} &= 2 \cos \alpha |A_L| |A_R| = \sin \vartheta \cos \phi, \\ S_2^{a,b} &= 2 \sin \alpha |A_L| |A_R| = \sin \vartheta \sin \phi, \\ S_3^{a,b} &= |A_L|^2 - |A_R|^2 = \cos \vartheta \end{aligned} \quad (3)$$

where $\alpha = \arg(A_R) - \arg(A_L)$ is the phase difference between A_L and A_R . Note that, for different parameters a and b , the same locations on the HOP describe different polarization states. In other

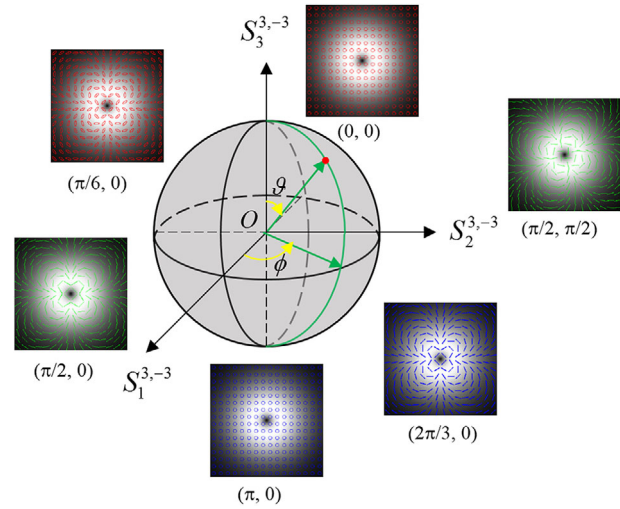


Figure 1. Schematic illustration of the HOP. The insets are the polarization maps of the HOP states located at the various positions on the HOP. Green, blue, and red labels represent the local linearly, right-handed elliptically, and left-handed elliptically polarized states, respectively.

words, different a and b correspond to different HOPs. Considering this point, the two parameters are labelled as superscript of the Stokes parameters. For example, we can map the polarization states for the HOP beams with $a = 3$ and $b = -3$ on the HOP by adopting the Stokes parameters ($S_1^{3,-3}, S_2^{3,-3}, S_3^{3,-3}$) as the Cartesian coordinates, as depicted in Figure 1.

The north ($\vartheta = 0$) and south ($\vartheta = \pi$) poles of the HOP represent left- and right-handed circularly polarized vortex beams, respectively. At the equator ($\vartheta = \pi/2$), the equation can be written as

$$E(\rho, \varphi) = A(\rho) (\cos(m\varphi + \phi/2) \hat{e}_x + \sin(m\varphi + \phi/2) \hat{e}_y) \exp(i\ell\varphi), \quad (4)$$

where $\hat{e}_x = \sqrt{2}(\hat{e}_L + \hat{e}_R)/2$ and $\hat{e}_y = -i\sqrt{2}(\hat{e}_L - \hat{e}_R)/2$ are the unit vectors in x and y directions. $m = (b - a)/2$ and $\ell = (b + a)/2$ represent the polarization order (PO) and the topological charge (TC), respectively. Such class of HOP beams are higher-order cylindrical vector vortex beams (CVVBs), and they become the well-known cylindrical vector beams (CVBs) when $\ell = 0$. For the generalized cases ($\vartheta \neq 0, \pi/2, \pi$), the northern and southern hemispheres represent spatially spirally variant left- and right-handed elliptically polarized beams. However, they cannot be described using certain PO and TC. Actually, any type of HOP beams possesses both vortex phase front and inhomogeneous polarization states. Thus, there exists interaction between SAM and OAM in the tightly focused fields of HOP beams.

To quantitatively study the AM properties in the tightly focused field, the electric fields of HOP beams focused under a high-NA focusing lens are calculated with the Richards–Wolf vectorial diffraction integral.^[38] In the focal plane, the formula of the

three electric field components (E_r, E_ϕ, E_z) are deduced under the cylindrical coordinates (r, ϕ, z), which read

$$\begin{aligned} E_r &= \cos\left(\frac{\theta}{2}\right) \exp\left(-i\frac{\phi}{2}\right) i^a e^{i(a+1)\phi} (I_a + I_{a+2}) \\ &\quad + \sin\left(\frac{\theta}{2}\right) \exp\left(i\frac{\phi}{2}\right) i^b e^{i(b-1)\phi} (I_b + I_{b-2}), \\ E_\phi &= \cos\left(\frac{\theta}{2}\right) \exp\left(-i\frac{\phi}{2}\right) i^{a+1} e^{i(a+1)\phi} (I_a - I_{a+2}) \\ &\quad + \sin\left(\frac{\theta}{2}\right) \exp\left(i\frac{\phi}{2}\right) i^{b-1} e^{i(b-1)\phi} (I_b - I_{b-2}), \\ E_z &= -\cos\left(\frac{\theta}{2}\right) \exp\left(-i\frac{\phi}{2}\right) i^{a+1} e^{i(a+1)\phi} I_{a+1} \\ &\quad - \sin\left(\frac{\theta}{2}\right) \exp\left(i\frac{\phi}{2}\right) i^{b-1} e^{i(b-1)\phi} I_{b-1} \end{aligned} \quad (5)$$

where

$$\begin{aligned} I_a &= -ikf \int_0^{\theta_{\max}} A(\theta) \sin\theta \cos^{1/2}\theta (1 + \cos\theta) \\ &\quad \times e^{ikz \cos\theta} J_a(kr \sin\theta) d\theta, \\ I_{a+2} &= -ikf \int_0^{\theta_{\max}} A(\theta) \sin\theta \cos^{1/2}\theta (1 - \cos\theta) \\ &\quad \times e^{ikz \cos\theta} J_{a+2}(kr \sin\theta) d\theta, \\ I_{a+1} &= -2ikf \int_0^{\theta_{\max}} A(\theta) \sin^2\theta \cos^{1/2}\theta e^{ikz \cos\theta} J_{a+1}(kr \sin\theta) d\theta, \\ I_b &= -ikf \int_0^{\theta_{\max}} A(\theta) \sin\theta \cos^{1/2}\theta (1 + \cos\theta) \\ &\quad \times e^{ikz \cos\theta} J_b(kr \sin\theta) d\theta, \\ I_{b-2} &= -ikf \int_0^{\theta_{\max}} A(\theta) \sin\theta \cos^{1/2}\theta (1 - \cos\theta) \\ &\quad \times e^{ikz \cos\theta} J_{b-2}(kr \sin\theta) d\theta, \\ I_{b-1} &= -2ikf \int_0^{\theta_{\max}} A(\theta) \sin^2\theta \cos^{1/2}\theta e^{ikz \cos\theta} J_{b-1}(kr \sin\theta) d\theta \end{aligned} \quad (6)$$

Here θ is the polar angle in the output plane of the focusing system with $\sin\theta_{\max} = \text{NA}$. $k = 2\pi/\lambda$ is the wave number of the monochromatic light with a wavelength of λ , and f is the focal length of the aplanatic lens. $J_l(\cdot)$ denotes the l -order Bessel function of the first kind. $A(\theta)$ is the initial amplitude profile of the circularly polarized vortex bases with the form of

$$A(\theta) = \left(\frac{\sqrt{2}\beta_0 \sin\theta}{\sin\theta_{\max}} \right) \exp\left(-\beta_0^2 \left(\frac{\sin\theta}{\sin\theta_{\max}} \right)^2 \right) \quad (7)$$

where β_0 is the ratio of the pupil radius and the beam waist radius. Throughout this paper, theoretical calculations are carried out under the conditions that $\text{NA} = 0.92$, $\lambda = 1.064 \mu\text{m}$, $f = 1.7 \text{ mm}$, and the ratio $\beta_0 = 1.2$.

According to the derived electric field components in the focal plane, the SAM and OAM densities can be calculated, which are 3D vectors to characterize the local spinning and orbiting energy

flux. For a time-harmonic light field with an angular frequency of $\omega = kc$ (c is the speed of light in vacuum), the time-averaged SAM and OAM densities are defined as^[39]

$$\begin{aligned} S &= \frac{\text{Im}[\epsilon(\mathbf{E}^* \times \mathbf{E}) + \mu(\mathbf{H}^* \times \mathbf{H})]}{4\omega}, \\ L &= \frac{\text{Im}[\epsilon(\mathbf{E}^* \cdot (\mathbf{r} \times \nabla) \mathbf{E}) + \mu(\mathbf{H}^* \cdot (\mathbf{r} \times \nabla) \mathbf{H})]}{4\omega} \end{aligned} \quad (8)$$

where ϵ and μ are the permittivity and permeability of a medium, and $*$ represents the complex conjugate of the variable. In light-matter interactions, because both the particle and the surrounding medium are commonly nonmagnetic, the particle predominantly reacts to the electric part of the light field. Hence, we focus on the SAM and OAM densities originated from the electric-field part.

3. Results and Discussions

The study of SOIs in highly focused HOP beams starts with the circularly polarized beams without incident OAM [Figure 2a1]. Figure 2a2–a4 presents intensity distributions in the focal plane of the focused left-handed circularly polarized beam as well as their corresponding phases (insets). Based on the electric field, local SAM density and OAM density distributions are further calculated. Figure 2a5–a7 shows the distributions of S_ϕ , S_z , and L_z , respectively. As expected, there exists longitudinal SAM component due to the incident SAM. However, although there is no OAM in the incident beam, we can observe the longitudinal OAM component in the focused field, which means the incident SAM partially converts into OAM under the highly focusing system. This phenomenon is termed as SOC and has been verified experimentally. Similarly, the SOC also occurs in highly focused right-handed circularly polarized beam but with an opposite longitudinal OAM component.

Furthermore, we introduce vortex phase into the circularly polarized beams and study the AM properties in the focused fields. Here we take the left-handed circularly polarized vortex beams with TC of $a = 2$ [Figure 2b1] and $a = -2$ [Figure 2c1] as an example. Their electric field components, local SAM density and longitudinal OAM density are presented in Figure 2b2–b7, c2–c7, respectively. Notably, the introduction of vortex phase results in changes of local SAM density compared with the circularly polarized beam. For further examination, the corresponding 1D local AM distributions along the x axis are given in Figure 3a–c. Both the SAM and OAM density components go away from the center with the increasing absolute value of TC. The signs of the azimuthally SAM and longitudinal OAM components vary synchronously with that of the TC. In particular, the focused left-handed circularly polarized beam ($a = 0$) has a positive longitudinal SAM component. However, it reverses from positive to negative when the vortex phase ($a = -2$) is introduced. It suggests that the incident OAM induces new local SAM density under high focusing, termed as localized OSC. The similar behaviors can be observed in the focused right-handed circularly polarized vortex beams, and the AM components have the same value but opposite signs compared with its left-handed circular counterpart, as shown in Figure 3d–f. Thus, both the SOC and OSC occur in the

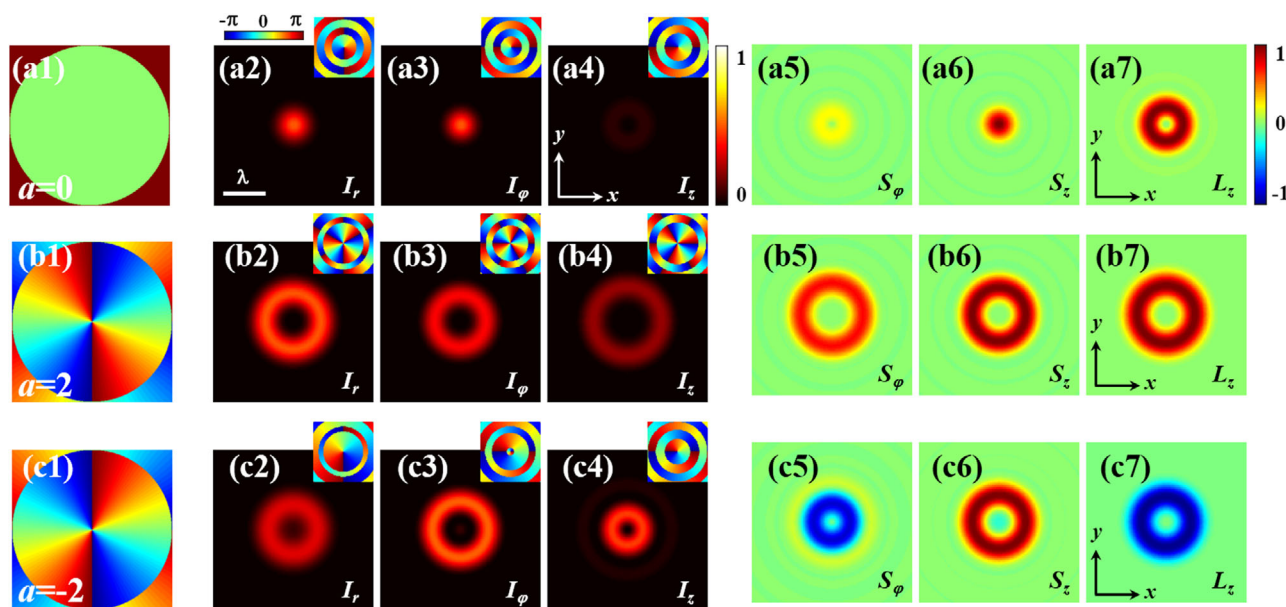


Figure 2. The phase maps of the incident left-handed circularly polarized vortex beams with TC of a1) $a = 0$ and b1) $a = 2$ and c1) $a = -2$. The intensity, phase (insets), SAM density, and OAM density profiles on the focal plane of the tightly focused left-handed circularly polarized vortex beams with TCs of a2–a7) $a = 0$ and b2–b7) $a = 2$ and c2–c7) $a = -2$.

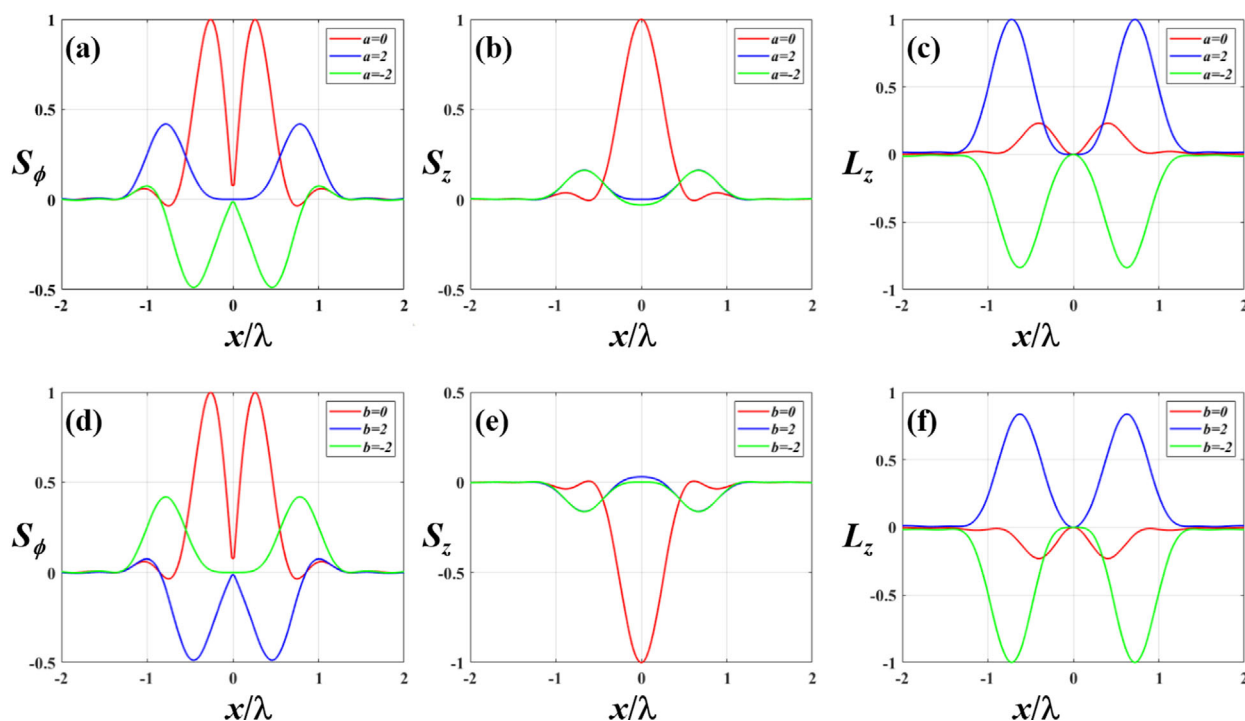


Figure 3. 1D azimuthal and longitudinal SAM, longitudinal OAM density distributions along the x -axis of the left-handed circularly polarized vortex beams a–c) with TC $a = 0, 2$, and -2 , and right-handed circularly polarized vortex beams d–f) with TC $b = 0, 2$ and -2 .

tightly focused circularly polarized vortex beams, and the interplay of SAM and OAM determines the distribution of AM density of the focused circularly polarized bases.

The circularly polarized states locate at the two poles of the HOP, and next we move on to the states located on the equa-

tor of the HOP. This kind of states are suppositions of the two bases with the same weighting, which are described by Equation (2). They are well-known higher-order cylindrical vector vortex modes that possess definite PO and the TC. To study their behaviors in terms of the SOIs, we take the third-order CVVBs

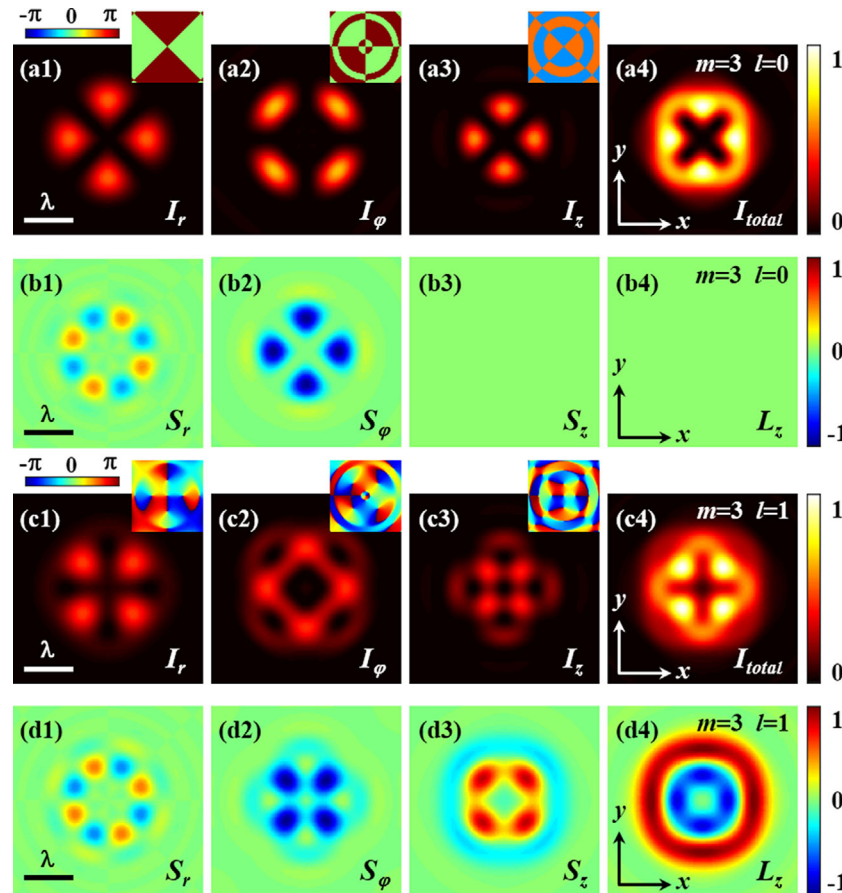


Figure 4. The intensity, phase (insets), SAM and OAM density profiles on the focal plane of the tightly focused third-order CVBs a1–b4) $m = 3$, $l = 0$, and third-order CVVBs c1–d4) $m = 3$, $l = 1$.

[$m = 3$ and $\phi = 0$ in the Equation (2)] as an example. The electric field components in the focal plane were calculated and local AM density distributions were obtained then. Particularly, we compared the SOI behaviors of focused beams with and without incident vortex phase, respectively. **Figure 4a,b** presents the calculated distributions of the electric field and AM density for the third-order CVBs, and **Figure 4c,d** shows the corresponding results of the third-order CVVBs with $l = 1$. We can observe transverse components in the SAM density, which exhibit petal-shaped profiles unlike the ring-like distributions in circularly polarized states. Note that, the total transverse SAM is zero due to its symmetry with respect to the origin. In particular, we observe no longitudinal component in both SAM and OAM densities in the focused CVBs. From the point of superposition, this is because the two bases have the same value but opposite signs for the longitudinal AM components. By contrast, the focused CVVBs possess the two longitudinal components simultaneously. The appearance of OAM component is as expected due to the introduction of incident vortex phase. However, the appearance of local SAM component cannot originate from the incident SAM, thus it should be induced by the incident OAM, which suggests the occurrence of localized OSC in this situation.

In addition, we find that the PO and TC also influence the distributions of SAM and OAM. **Figure 5** presents the calculated results about the SAM and OAM density distributions in

focused CVVBs with different POs and TCs. The magnitudes of SAM exhibit petal-shaped patterns and the radial component has $4|m - 1|$ lobes along the azimuthal direction [first column of **Figure 5**], whereas the azimuthal component has $2|m - 1|$ lobes [second column of **Figure 5**]. In contrast, the longitudinal SAM component is determined by the PO and TC together, and it also applies to the OAM.

According to Equation (2), the PO and TC of CVVBs are determined by the TCs (a , b in Equation (1)) of the two superposition bases. Thus, changing either PO or TC actually changes the vortex phases of the two bases. As we revealed above, SOC and OSC occur in the tightly focused circularly polarized vortex states, and changing the incident vortex phase affects both the OAM and SAM densities in the focal plane. Although there is no SAM in the incident field, the AM density of the CVVBs, as the superposition states, changes accordingly with the vortex phases of two bases.

Finally, we turn to the states located on the northern and southern hemispheres excluding the two poles. These states are superpositions of the two circularly polarized bases with different weightings. For simplicity, we focus on the case of $a = -b$ in Equation (1). In this case, the two bases have the opposite OAM. Similarly, we calculated electric fields of the superposition states and study their behaviors of the SOI in the focal plane. **Figure 6a,b** shows a typical example, the third-order spatially spirally

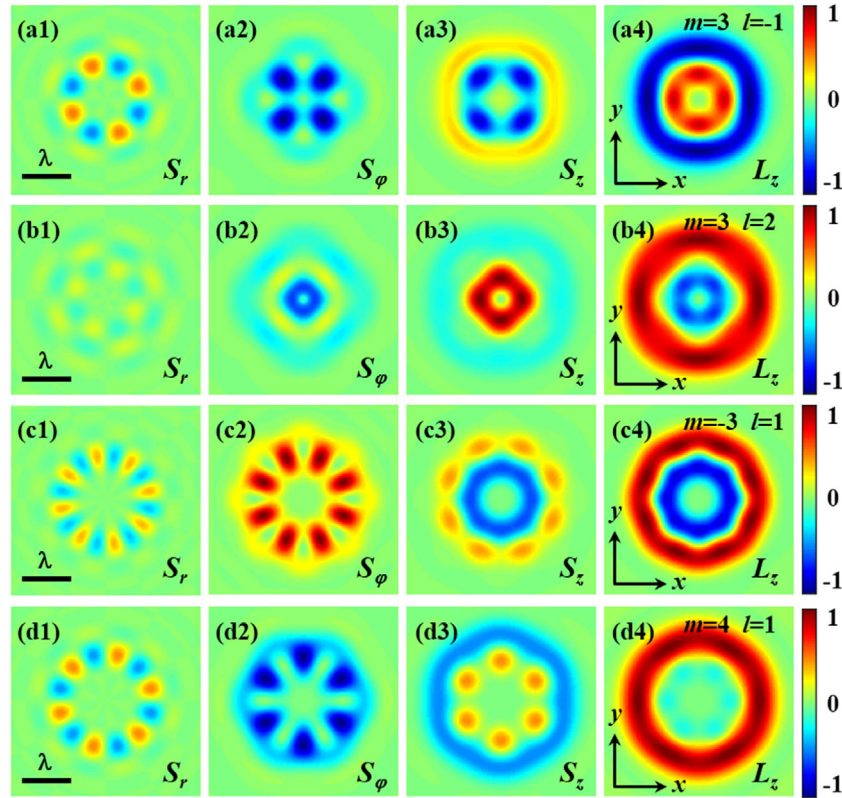


Figure 5. The intensity, phase (insets), SAM and OAM density profiles on the focal plane of the tightly focused higher-order CVVBs with a1–b4) $m = 3$, $l = -1$, b1–b4) $m = 3$, $l = 2$, c1–c4) $m = -3$, $l = 1$, d1–d4) $m = 4$, $l = 1$.

left-handed elliptically polarized beams with the parameters of $\vartheta = \pi/6$, $\phi = 0$. Distinguished from the CVBs in Figure 4a,b, such beams possess both SAM and OAM longitudinal components in the focused field. Note that, the longitudinal AM components of the two bases have the same value but opposite signs. Thus, the different weightings in the superposition lead to the appearance of the longitudinal AM components. Our study further discusses the various states located in the same longitude line of the HOP. We mainly calculated the longitudinal AM components with the varying longitude angles, and their 1D distributions along the x axis are given in Figure 6c,d. The states located on both hemispheres have longitudinal AM components and their magnitudes vary with longitude angles. Besides, their signs are opposite for the southern and northern hemispheres. Mathematically, the change of the longitudinal AM density originates from the varying weightings of two bases. Physically, it can be attributed to the interplay between SAM and OAM in tightly focusing system. There exist both SAM and OAM in the incident fields before being focused, and SOC and OSC simultaneously occur. As a result, the interplay determines the properties of the focused fields.

To figure out the quantitative conversion between SAM and OAM of HOP beams under tight focusing, we analyze the electric components, SAM, OAM, and total AM densities of the fields before and after focusing. For easy identification, we use the superscripts i and o to indicate the components before and after focusing, respectively. According to Equation (1), the electric field

components of the incident field (E_x^i , E_y^i , E_z^i) have the form of

$$\begin{aligned} E_x^i &= \frac{\sqrt{2}}{2} \cos\left(\frac{\vartheta}{2}\right) A(\rho) \exp\left(-i\frac{\phi}{2}\right) \exp(ia\varphi) \\ &\quad + \frac{\sqrt{2}}{2} \sin\left(\frac{\vartheta}{2}\right) A(\rho) \exp\left(i\frac{\phi}{2}\right) \exp(ib\varphi), \\ E_y^i &= \frac{i\sqrt{2}}{2} \cos\left(\frac{\vartheta}{2}\right) A(\rho) \exp\left(-i\frac{\phi}{2}\right) \exp(ia\varphi) \\ &\quad - \frac{i\sqrt{2}}{2} \sin\left(\frac{\vartheta}{2}\right) A(\rho) \exp\left(i\frac{\phi}{2}\right) \exp(ib\varphi), \\ E_z^i &= 0, \end{aligned} \quad (9)$$

We then deduce the formula of the orbital, spin and total AM flow densities in the incident field, which reads

$$L_z^i = \frac{\epsilon_1 A^2(\rho) \left(a \cos^2\left(\frac{\vartheta}{2}\right) + b \sin^2\left(\frac{\vartheta}{2}\right) \right)}{4\omega}, \quad L_T^i = 0 \quad (10)$$

$$S_z^i = \frac{\epsilon_1 A^2(\rho) \left(\cos^2\left(\frac{\vartheta}{2}\right) - \sin^2\left(\frac{\vartheta}{2}\right) \right)}{4\omega}, \quad S_T^i = 0 \quad (11)$$

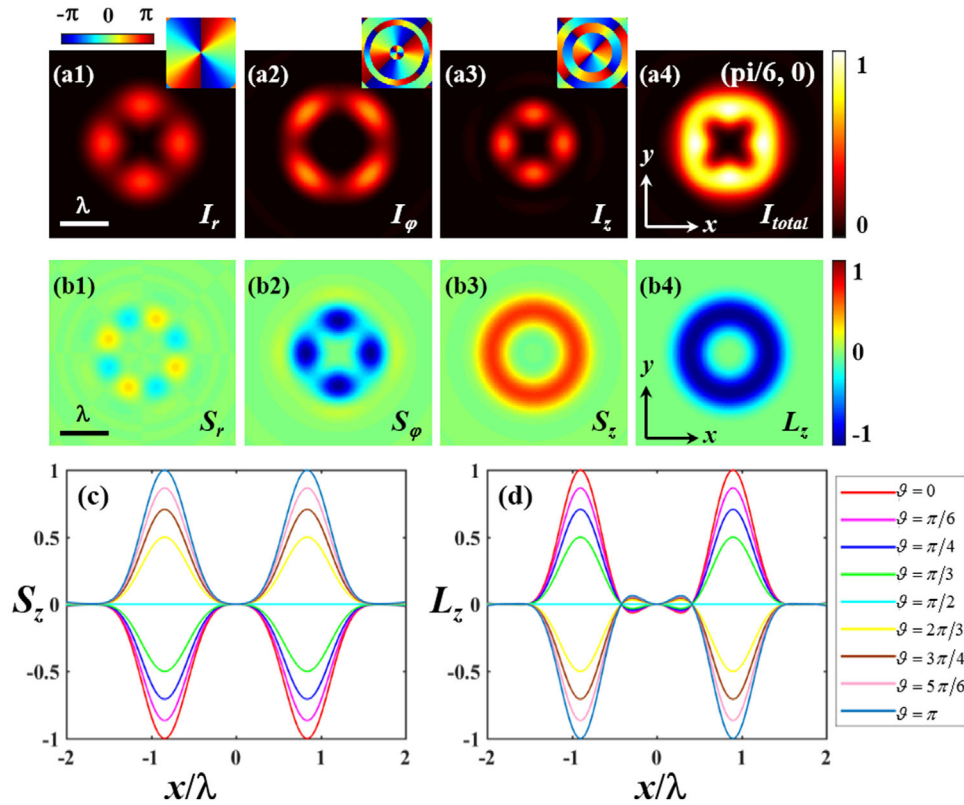


Figure 6. The intensity, phase (insets), SAM, and OAM density profiles on the focal plane of the tightly focused third-order spatially spirally left-handed elliptically polarized beams in the Northern Hemisphere of the HOP a1–b4) with $\theta = \pi/6$, $\phi = 0$. c,d) 1D distributions of the longitudinal SAM and OAM density components along the x axis of the HOP beams with various longitude angles located at the HOP.

$$P_z^i = L_z^i + S_z^i = \frac{\epsilon_1 A^2(\rho) \left((a+1) \cos^2\left(\frac{\theta}{2}\right) + (b-1) \sin^2\left(\frac{\theta}{2}\right) \right)}{4\omega} \quad (12)$$

It indicates that the incident fields have the pure longitudinal OAM (L_z^i) and SAM (S_z^i) flow densities, and both the transverse OAM (L_r^i) and SAM (S_r^i) are zero. The magnitude of the S_z^i is determined by the longitude angle θ in the HOP, whereas the L_z^i is determined by the longitude angle θ and the TCs of the two superposition bases as well as the total AM (P_z^i).

Once focused with a high-NA lens, the partial rays refract and converge at the focal point and have the nonparaxial \mathbf{k} -vectors characterized by the converging angle $\theta = \arcsin(r/f)$. The components of the refracted field (E_x^o , E_y^o , E_z^o) at the focusing plan can be calculated by the Debye–Wolf theory as

$$\begin{aligned} E_x^o &= \frac{\sqrt{2}}{4} \cos\left(\frac{\theta}{2}\right) A(\rho) \exp\left(-i\frac{\phi}{2}\right) \\ &\times \left[(1 + \cos\theta) - (1 - \cos\theta) e^{i2\varphi} \right] \exp(i a \varphi) \\ &+ \frac{\sqrt{2}}{4} \sin\left(\frac{\theta}{2}\right) A(\rho) \exp\left(i\frac{\phi}{2}\right) \\ &\times \left[(1 + \cos\theta) - (1 - \cos\theta) e^{-i2\varphi} \right] \exp(i b \varphi), \end{aligned}$$

$$\begin{aligned} E_y^o &= \frac{i\sqrt{2}}{4} \cos\left(\frac{\theta}{2}\right) A(\rho) \exp\left(-i\frac{\phi}{2}\right) \\ &\times \left[(1 + \cos\theta) + (1 - \cos\theta) e^{i2\varphi} \right] \exp(i a \varphi) \\ &- \frac{i\sqrt{2}}{4} \sin\left(\frac{\theta}{2}\right) A(\rho) \exp\left(i\frac{\phi}{2}\right) \\ &\times \left[(1 + \cos\theta) + (1 - \cos\theta) e^{-i2\varphi} \right] \exp(i b \varphi), \\ E_z^o &= -\frac{\sqrt{2}}{2} \cos\left(\frac{\theta}{2}\right) A(\rho) \exp\left(-i\frac{\phi}{2}\right) \sin\theta \exp(i(a+1)\varphi) \\ &- \frac{\sqrt{2}}{2} \sin\left(\frac{\theta}{2}\right) A(\rho) \exp\left(i\frac{\phi}{2}\right) \sin\theta \exp(i(b-1)\varphi) \quad (13) \end{aligned}$$

The orbital, spin, and total AM flow densities on the back plane of the lens can be calculated with Equation (3), which read

$$\begin{aligned} L_z^o &= \frac{\epsilon_1 A^2(\rho) \left((a+1 - \cos\theta) \cos^2\left(\frac{\theta}{2}\right) + (b + \cos\theta - 1) \sin^2\left(\frac{\theta}{2}\right) \right)}{4\omega}, \\ L_r^o &= 0 \end{aligned} \quad (14)$$

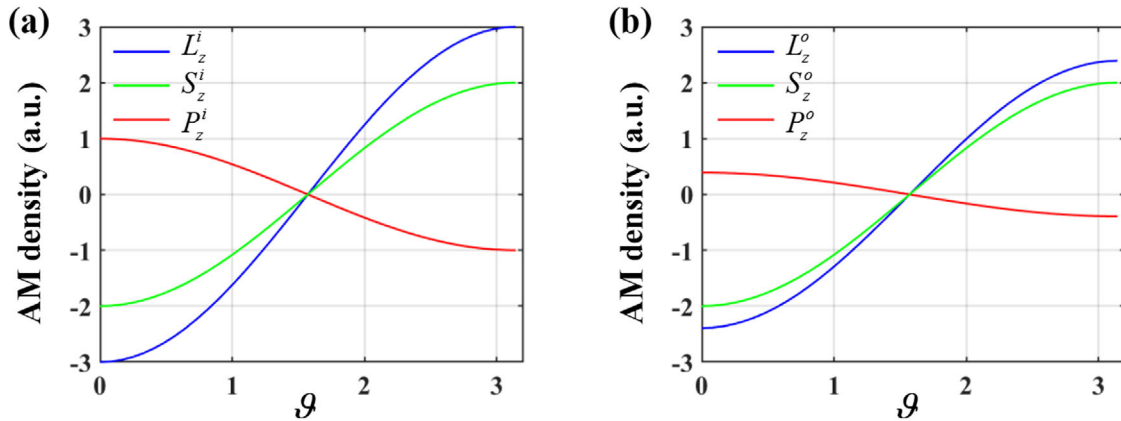


Figure 7. Longitudinal OAM density, longitudinal SAM density, and total AM density of the third-order Poincaré sphere beams varying with the longitudinal angle before a) and after b) focusing.

$$S_z^o = \frac{\epsilon_1 A^2(\rho) \cos \theta \left(\cos^2 \left(\frac{\theta}{2} \right) - \sin^2 \left(\frac{\theta}{2} \right) \right)}{4\omega},$$

$$S_T^o = 0 \quad (15)$$

$$P_z^o = L_z^o + S_z^o = \frac{\epsilon_1 A^2(\rho) \left((a+1) \cos^2 \left(\frac{\theta}{2} \right) + (b-1) \sin^2 \left(\frac{\theta}{2} \right) \right)}{4\omega} \quad (16)$$

The focused field has an extra longitudinal OAM (L_z^o) and SAM (S_z^o) compared with the incident field, and both the transverse OAM (L_T^o) and SAM (S_T^o) are zero. In fact, the extra ones come from the spin-orbit conversion under the tight focusing system. It should be noted that the OSC is different from SOC. The incident SAM is indeed converted into OAM in the focused field, while the incident OAM is not converted into SAM but induces redistribution of local SAM density. After refraction, the longitudinal SAM density is modulated by $\cos \theta$, and the longitudinal OAM density has a complementary change with the longitudinal SAM density. In contrast, the total AM densities of the focused field and incident field are the same ($P_z^o = P_z^i$), which verifies the AM conservation. For an intuitive examination, we present the curves of the changing AM densities as a function of longitude angle ϑ in **Figure 7** for typical third-order Poincaré sphere beams with $\theta = \sin(NA)$. It shows that the absolute magnitudes of the SAM and OAM densities vary with the ϑ before and after focusing. The amounts of the extra SAM and OAM in the refracted field are determined by the weightings between the two bases and the converging angle of the focusing system together. Note that, the weightings between the two bases depend on the sphere's spherical coordinates (ϑ, ϕ) of the HOP, which refer to various HOP beams. That means the HOP quantitatively illustrates the interconversion between SAM and OAM in the tightly focused HOP beams.

4. Conclusions

In conclusion, we have theoretically studied the complex focal properties of various HOP beams, and revealed the interplay be-

tween SAM and OAM in the focused field. The amounts of the transformed SAM and OAM are determined by the weightings between the two circularly polarized bases and the converging angle of the focusing system together. Additionally, the conversions for various HOP beams can be quantitatively represented according to their coordinates on the HOP. Overall, the interplay between SAM and OAM determines the complex behaviors in the focused field of the HOP beams. Mathematically, the behaviors can be explained based on the superposition of two circular polarization vortex bases. Thus, arbitrary control of the local SAM and OAM densities can be achieved by tuning the superposition weightings, paving a way to control the SOIs in the focused field. The SOIs of light represent a new paradigm that provides physical insight and describes the behavior of polarized light at subwavelength scales. Thus, our findings are expected to benefit applications where tight focusing is involved, such as optical trapping and super-resolution microscopy.

Acknowledgements

This work was supported by the National Natural Science Foundation of China (Grant Nos. 61535011 and 11704369 and 11974333).

Conflict of Interest

The authors declare no conflict of interest.

Keywords

higher-order Poincaré sphere beams, spin-orbit interaction, tight focusing

Received: March 6, 2020

Revised: May 25, 2020

Published online:

[1] J. H. Poynting, *Proc. R. Soc. London, Ser. A* **1909**, 82, 560.

[2] A. O'neil, I. MacVicar, L. Allen, M. Padgett, *Phys. Rev. Lett.* **2002**, 88, 053601.

- [3] K. Y. Bliokh, J. Dressel, F. Nori, *New J. Phys.* **2014**, *16*, 093037.
- [4] K. Y. Bliokh, E. A. Ostrovskaya, M. A. Alonso, O. G. Rodríguez-Herrera, D. Lara, C. Dainty, *Opt. Express* **2011**, *19*, 26132.
- [5] M. Neugebauer, P. Banzer, T. Bauer, S. Orlov, N. Lindlein, A. Aiello, G. Leuchs, *Phys. Rev. A* **2014**, *89*, 013840.
- [6] M. Onoda, S. Murakami, N. Nagaosa, *Phys. Rev. Lett.* **2004**, *93*, 083901.
- [7] L. Du, A. Yang, A. V. Zayats, X. Yuan, *Nat. Phys.* **2019**, *15*, 650.
- [8] S. Fu, C. Guo, G. Liu, Y. Li, H. Yin, Z. Li, Z. Chen, *Phys. Rev. Lett.* **2019**, *123*, 243904.
- [9] P. Yu, Q. Zhao, X. Hu, Y. Li, L. Gong, *Appl. Phys. Lett.* **2018**, *113*, 121102.
- [10] K. S. Grigoriev, I. A. Perezhogin, V. A. Makarov, *Opt. Lett.* **2018**, *43*, 5182.
- [11] X. Ling, X. Zhou, K. Huang, Y. Liu, C.-W. Qiu, H. Luo, S. Wen, *Rep. Prog. Phys.* **2017**, *80*, 066401.
- [12] C. P. Jisha, A. Alberucci, *Opt. Lett.* **2017**, *42*, 419.
- [13] R. C. Devlin, A. Ambrosio, N. A. Rubin, J. B. Mueller, F. Capasso, *Science* **2017**, *358*, 896.
- [14] F. Cardano, L. Marrucci, *Nat. Photonics* **2015**, *9*, 776.
- [15] K. Y. Bliokh, A. Y. Bekshaev, F. Nori, *Nat. Commun.* **2014**, *5*, 3300.
- [16] J. P. Balthasar Mueller, N. A. Rubin, R. C. Devlin, B. Groever, F. Capasso, *Phys. Rev. Lett.* **2017**, *118*, 113901.
- [17] S. Divitt, W. Zhu, C. Zhang, H. J. Lezec, A. Agrawal, *Science* **2019**, *364*, 890.
- [18] I. S. Osborne, *Science* **2019**, *365*, 40.
- [19] K. Wang, J. G. Titchener, S. S. Kruk, L. Xu, H. P. Chung, M. Parry, Kravchenko, II, Y. H. Chen, A. S. Solntsev, Y. S. Kivshar, D. N. Neshev, A. A. Sukhorukov, *Science* **2018**, *361*, 1104.
- [20] S. Colburn, A. Zhan, A. Majumdar, *Sci. Adv.* **2018**, *4*, eaar2114.
- [21] Z.-L. Deng, G. Li, *Materials Today Physics* **2017**, *3*, 16.
- [22] P. Woźniak, I. De Leon, K. Höflich, G. Leuchs, P. Banzer, *Optica* **2019**, *6*, 961.
- [23] M. Babiker, C. R. Bennett, D. L. Andrews, L. C. Davila Romero, *Phys. Rev. Lett.* **2002**, *89*, 143601.
- [24] M. Friesse, T. Nieminen, N. Heckenberg, H. Rubinsztein-Dunlop, *Nature* **1998**, *394*, 348.
- [25] L. Paterson, M. MacDonald, J. Arlt, W. Sibbett, P. Bryant, K. Dholakia, *Science* **2001**, *292*, 912.
- [26] P. Shi, L. Du, X. Yuan, *Opt. Express* **2018**, *26*, 23449.
- [27] Y. Bai, M. Dong, M. Zhang, Y. Yang, *Nanoscale Res. Lett.* **2019**, *14*, 252.
- [28] R. Chen, K. Agarwal, C. J. Sheppard, X. Chen, *Opt. Lett.* **2013**, *38*, 3111.
- [29] Y. Zhao, J. S. Edgar, G. D. Jeffries, D. McGloin, D. T. Chiu, *Phys. Rev. Lett.* **2007**, *99*, 073901.
- [30] Z. e. Bomzon, M. Gu, J. Shamir, *Appl. Phys. Lett.* **2006**, *89*, 241104.
- [31] Y. Zhao, D. Shapiro, D. McGloin, D. T. Chiu, S. Marchesini, *Opt. Express* **2009**, *17*, 23316.
- [32] P. Yu, Q. Zhao, X. Hu, Y. Li, L. Gong, *Opt. Lett.* **2018**, *43*, 5677.
- [33] L. Han, S. Liu, P. Li, Y. Zhang, H. Cheng, J. Zhao, *Phys. Rev. A* **2018**, *97*, 053802.
- [34] M. Li, Y. Cai, S. Yan, Y. Liang, P. Zhang, B. Yao, *Phys. Rev. A* **2018**, *97*, 053842.
- [35] G. Milione, H. I. Sztul, D. A. Nolan, R. R. Alfano, *Phys. Rev. Lett.* **2011**, *107*, 053601.
- [36] D. Naidoo, F. S. Roux, A. Dudley, I. Litvin, B. Piccirillo, L. Marrucci, A. Forbes, *Nat. Photonics* **2016**, *10*, 327.
- [37] M. Dong, X. Lu, C. Zhao, Y. Cai, Y. Yang, *Opt. Express* **2018**, *26*, 33035.
- [38] B. Richards, E. Wolf, *Proc. R. Soc. London, Ser. A* **1959**, *253*, 358.
- [39] A. Aiello, P. Banzer, M. Neugebauer, G. Leuchs, *Nat. Photonics* **2015**, *9*, 789.